An application of a reality-based approach for the generation of masonry cross vaults FE block models

Structures 65 (2024) 106638

Contents lists available at ScienceDirect

Structures

journal homepage: www.elsevier.com/locate/structures

An application of a reality-based approach for the generation of masonry cross vaults FE block models

Marco Alforno [a,*], Alessia Monaco [a], Fiammetta Venuti [a], Chiara Calderini [b], Giulia Sammartano [a], Giacomo Patrucco [a], Antonia Spanó [a]

[a] Politecnico di Torino, Department of Architecture and Design, Viale Mattioli 39, Torino, 10125, Italy
[b] Universitá di Genova, Department of Civil, Chemical and Environmental Engineering, via Montallegro 1, Genova, 16145, Italy

ARTICLE INFO

Keywords:
Masonry vaults
3D modelling
LiDAR
Digital photogrammetry
Masonry pattern
FE block model

ABSTRACT

In recent years, the synergy between Geomatics and Structural Engineering has opened new frontiers in the analysis of the built heritage. In particular, the possibility of using reality-based models as starting data to develop structural models has become increasingly appealing to take into account some aspects that are usually neglected in the analysis of historical masonry constructions, such as the as-built deformed geometry and the block arrangement. The proposed approach is based on an integrated 3D metric survey campaign, that allows dense point clouds with RGB information to be obtained through LiDAR acquisitions and the contribution of photogrammetric surveys. These data are subsequently used for adaptive NURBS modelling to develop Finite Element micro-Models. This approach is applied to two cross vaults belonging to the portico of the Palazzata di Vicoforte in Piedmont, Italy, characterized by very similar macro-geometry, but different brick pattern. The developed FE models are analysed under differential settlement of the abutments, namely opening, vertical and shear settlement. The results are also compared with those obtained in a previous numerical campaign on ideal cross vaults of similar macro-geometry: the shear settlement is assumed for comparison, revealing the importance of accurate geometrical modelling at different scales.

1. Introduction

In recent years, the synergy between Geomatics and Structural Engineering has opened new frontiers in the modelling and analysis approaches for the built heritage, as testified by several interdisciplinary studies (e.g., [1–4]). Actually, the huge complexity characterizing historical buildings makes it mandatory a multidisciplinary approach to deal with documentation, conservation, strengthening and restoration of the architectural heritage. In this framework, the geometrical complexity can be efficiently analysed thanks to the non-invasive instruments and techniques provided by Geomatics methods.

In fact, we are witnessing a widespread and intense improvement in terms of technologies for data capturing as well as their sensors performance and processing algorithms, which are increasingly effective and implemented in commercial software [5]. The research sector concerning the modelling phase, however, is still under development, looking for automatism, effectiveness of final results, and adaptability of user-oriented solutions. In nowadays' framework, fusion-based strategies for point clouds capturing benefit from range-based sensors, such as laser scanning technologies, and image-based approaches following multi-scale and multi-band photogrammetric pipelines. They represent the most recognized and accurate solution concerning 3D metric digitization of historical buildings and masonries [6,7]. In particular, the integration of these methods allows the connection between 3D digital geometries characterized by very high spatial resolution and the radiometric information derived from image-based photogrammetric techniques, enabling an enhanced reading of elements that depend on both the geometry and radiometry (i.e. shape and colour) of an architectural asset (e.g., material consistency or masonry texture) for documentation, inspection and monitoring [8–10]. These approaches allow to obtain reality-based geometrical 3D models characterized by a pre-established very high accuracy and level of detail, as well as extreme data density.

Reality-based models generated from dense point clouds and derived from as-built modelling approaches can be used as primary data to develop structural models for the analysis of the surveyed object with different ad-hoc solutions, usually based on the integration of multi-source data [11].

The proposed methodologies approaching the reality-based modelling phase allow to consider some aspects that are usually neglected in the structural analysis of masonry structures, e.g., the as-built geometry

* Corresponding author.
E-mail address: marco.alforno@polito.it (M. Alforno).

https://doi.org/10.1016/j.istruc.2024.106638
Received 15 December 2023; Received in revised form 11 April 2024; Accepted 23 May 2024
Available online 30 May 2024

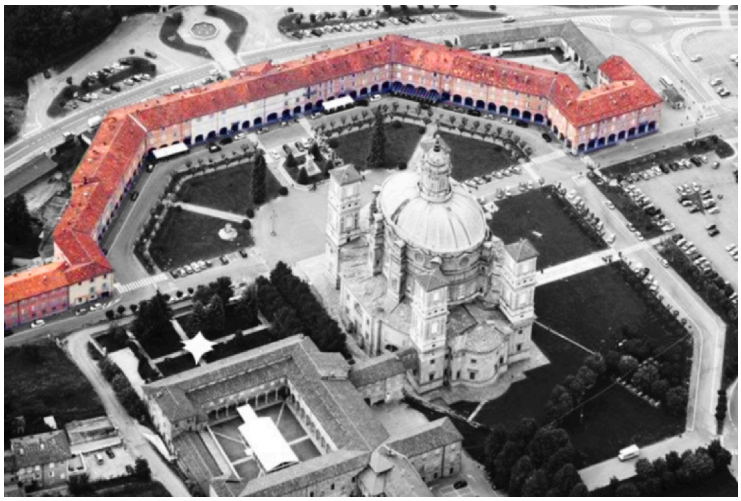

Fig. 1. The Sanctuary of Vicoforte and the Palazzata (in colour). (For interpretation of the references to colour in this figure, the reader is referred to the web version of this article.)

in its deformed state and the block arrangement [12]. With respect to this latter feature, the development of FE block models is the most efficient way to accurately describe the real brick arrangement and to account for its effects on the structural behaviour [12–14].

The direct generation of FE models for structural analysis from the geometric model derived from dense point cloud – so-called *scan-to-FEM* approach – has been investigated in several recent studies (e.g., [15–17]). The FE models derived from the available scan-to-FEM procedures are generally developed according to the macro-modelling approach, where masonry is considered as a homogeneous continuous material. The possibility to apply scan-to-FEM for the generation of FE block models is still an open research issue [18–20]. For this reason, in this study FE block models will be generated according to a manual procedure.

This study investigates the implications of applying the reality-based modelling approach to a case study: the Palazzata di Vicoforte in Piedmont, Italy. First, a 3D metric survey campaign has been carried out along the portico and the survey planning mainly refers to their masonry vaults. The strategy exploits the very high spatial resolution of the 3D model derived from LiDAR data as well as the radiometric contribution integrated by the photogrammetric approach. Hence, it was possible to develop a hybrid strategy to achieve an optimized 3D dense surface useful as the starting point for subsequent as-built discrete modelling based on NURBS, the preliminary data for the structural models. Finally, Finite Element models are developed of two cross vaults characterized by very similar macro-geometry, but different brick pattern. The models are tested under differential settlements at the abutments and results are compared with those obtained on similar vaults of ideal geometry. The scope is highlighting which is the influence of accurate real geometry, usually characterized by imperfections, in the assessment of the mechanical response of vaulted structures with different masonry block layouts.

The paper develops as follows: Section 2 describes the chosen case study; Sections 3 and 4 illustrate the 3D metric survey and data post-processing; Sections 5 and 6 are devoted to structural modelling and analysis, respectively, while conclusions are discussed in Section 7.

2. Description of the case study

The proposed approach is applied to the Palazzata di Vicoforte in Piedmont, Italy (Fig. 1), which is located aside the Santuario Regina Montis Regalis di Vicoforte (also briefly known as Santuario di Vicoforte). The latter is a monumental church located in Vicoforte, Piedmont, northern Italy, known for being covered by the largest elliptical dome in the world. The Palazzata is entirely constructed in brickworks, with the exception of stone pillars [21]. It consists of three main wings, one central and two lateral, built in different centuries starting from 1597, as shown in Fig. 1. The ground floor is characterized by a long portico facing the Sanctuary, made of a sequence of cross vaults of approximately 3.2 metres of span. Most of the vaults do not have plasterwork at the intrados surface, making the brick arrangement visible. All vaults are built with bricks, regular in shape and arranged in a diagonal or radial pattern with respect to the head arches (Fig. 2).

For the scope of this study, only the vaults of the central wing are considered. Three blocks of four vaults each are defined, as shown in Fig. 3. The vaults of block 3 were built in the 17th century [21] and are visibly different from the vaults of the other two blocks. They are cross vaults, arranged with an irregular diagonal pattern, whose groins tend to disappear in the central area of the vaults (transitioning into a sail-like vault). On the contrary, the other two blocks (both dating 18th century) show more traditional cross vaults, qualitatively similar in blocks 1 and 2, however arranged with a radial pattern in block 1 and a diagonal pattern in block 2.

3. Geometric survey

The up-to-date research direction in reality-based approaches follows at least one main crucial requirement: the optimization of procedures in the acquisition and modelling phases. This is related to both the nature of 3D data and to the modelling algorithms. On one hand, one of the challenging tasks is to optimize the huge number of redundant points captured by static Terrestrial Laser Scanning (TLS) in the generation phase for the surface-based or object-based modelling. In this sense, new rapid approaches have been developed and investigated in recent years based on portable scanning or imaging systems. These techniques generate, depending on the application contexts, manageable and medium-density 3D point data (e.g. SLAM-based point clouds, 360° camera acquisition, videogrammetry). On the other hand, for the well-known time-consuming modelling phases based on Boundary-Representation methods (B-rep) [22], the automation of surface and object-based generation has been faced with different solutions such as semantic segmentation, classification and parametric approaches based on point cloud data [23] and their Grades of Generation, as proposed in [24].

This section presents the data fusion strategy, based on the 3D models derived from LiDAR point clouds and the added-value from the metric products achieved following photogrammetric approach. These data represent the starting point for subsequent reality-based NURBS discrete modelling and configuration of elements for structural analyses.

Fig. 2. View of two different 18th century vaults of the portico, with radial masonry pattern (right) and diagonal pattern (left).

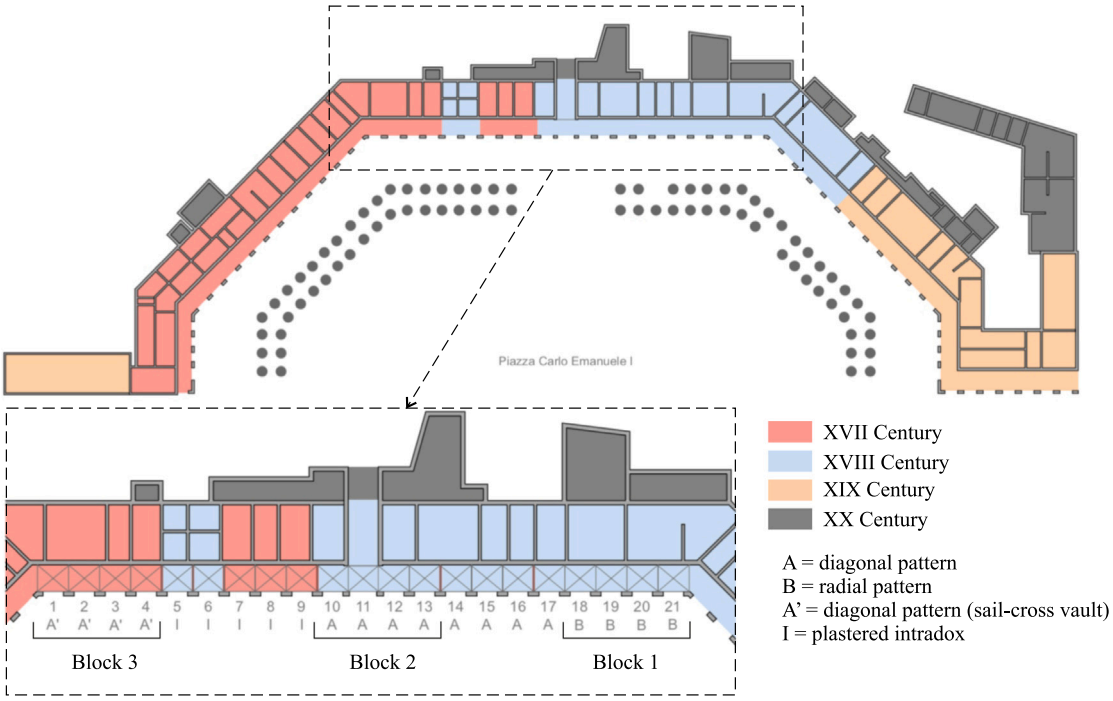

Fig. 3. Scheme of the Palazzata, identification of construction stages and of three blocks subject to the survey campaign. (For interpretation of the references to colour in this figure, the reader is referred to the web version of this article.)

The 3D metric survey of the Palazzata portico was performed following the presented workflow. A crucial role is played by the automation process in data acquisition thanks to digital technologies approaches, which speed up the on-site data collection phase. In the subsequent processing phases, the role of the operator is necessary in software interface-assisted processes in order to elaborate both the 3D scans co-registration and the photogrammetric pipeline, as well as the point cloud-based modelling phase. First, a topographic network has been measured in order to provide a common reference system and a metric control to the subsequently acquired range-based and image-based data. A set of topographic vertices defining the network have been manually measured by total station and then a couple of GNSS (Global Navigation Satellite Systems) receivers have been used for baseline measurements and absolute georeferencing in WGS84 system. The network has been adjusted with millimetric accuracy in order to guarantee a controlled and limited error propagation on the object measured points and on the global model accuracy. Therefore, a set of detail points was measured using the total station from the vertices positions to be used as control points. Twelve LiDAR scans have been collected using a Faro Focus3D X 330 phase shift laser scanner (15 min per scans, range+image data). The high overlap between adjacent scans in the scans plan project facilitates the subsequent co-registration procedures implemented on scan management software, that automatically calculates relative scans positions according to the scans acquisition configuration, their spatial similarity and 3D feature. The LiDAR scans have been oriented in the same reference system determined by the previously measured topographic network using the following strategy in the registration phase. Initially, the scans were aligned using an ICP-based (Iterative Closest Point) approach, exploiting the high overlap between adjacent point clouds. The discrepancies observed among the registered scans at the end of this preliminary procedure were millimetre-level (approximately, a mean value of approximately 2 mm was achieved). Subsequently, the block of scans was rigidly rototraslated in the reference system using a set of measured control

(a) (b)

Fig. 4. From LiDAR Point Clouds of the Palazzata (a) to mesh (b).

Table 1
RMSEs on GCPs and CPs.

	X [m]	Y [m]	Z [m]	XYZ [m]
GCPs (n°15)	0.003	0.002	0.002	0.004
CPs (n°7)	0.002	0.002	0.004	0.005

points (natural points or checkboard targets manually positioned on scans views). In this case the observed accuracy is approximately 5 mm.

Afterwards, a close-range photogrammetric survey has been carried out in order to collect high-resolution digital images of the selected cross vaults. A Digital Single Lens Reflex (DSLR) camera Canon EOS 5DSR, equipped with a Zeiss 25 mm lens, was set in nadiral configuration in relation to the vaults and mounted on a tripod. Then, two photogrammetric strips have been manually acquired in almost 30 min from a shooting distance ≈ 3.2 m with an estimated overlapping of 90% and an average Ground Sample Distance (GSD) of 0.5 mm. Then, the photogrammetric blocks have been processed following a standard SfM-based (Structure-from-Motion) pipeline [25] implemented and semi-automated into Agisoft Metashape GUI: Interior Orientation (determination of the intrinsic parameters of the camera); Relative Orientation of the images and generation of a sparse cloud of tie points; Absolute Orientation using a set of Ground Control Points (GCPs) homogeneously distributed on the surveyed surface and measured with the total station; accuracy evaluation using a set of Control Points (CPs). The observed Root Mean Square Errors (RMSEs) are millimetre-level for both GCPs and CPs, as reported in Table 1.

4. Data post-processing

Starting from the obtained reality-based 3D point cloud data (Fig. 4a) a very accurate as-built NURBS modelling has been performed following experimented and validated workflows based on profile extraction and curve interpolation. [11]. The software interface used for the implementation is Rhinoceros® platform (Fig. 4b). First, a high-detail mesh has been calculated by interpolation from the LiDAR point clouds (Fig. 2c). This dense triangulated model represents the intrados surface of the vaults, and the surfaces of walls and pillars facing the interior of the portico. The mesh triangles dimensions can be sub-millimetric, hence it is possible to detect the mortar joints from the models. To improve the detection of the mortar joints, the radiometric information obtained from the photogrammetric survey has been projected onto the mesh, texturing the surface of the hybrid 3D model.

These models can be used for different purposes: analysis of geometrical deviations from a hypothetical undeformed configuration in order to perform damage assessment at the macro-scale [26]; cracks detection in order to perform damage assessment at a micro-scale; generation of numerical models for structural analysis. With regard to crack-pattern detection, the survey can be performed on ortho-photos of the intrados surfaces generated from the texturized models. Fig. 8 shows an example of crack pattern detection performed on the three surveyed blocks. In particular, the cracks have been categorized in cracks along joints and cracks through bricks on the basis of their location. Moreover, cracks along joints are further divided into minor and major cracks on the basis of the observed thickness. The crack types depicted in the figure have been detected through a visual analysis of the ortho-photos, without automated procedures. It can be observed that the three sets of vaults display different type of cracks: block 1 (radial cross vaults) is mainly interested by minor cracks along mortar joints that are parallel to the groins; in block 2 (diagonal cross vault) the prevalent crack type occurs through bricks; block 3 (diagonal cross-sail vault) appears to be the most damaged part of the porticos, showing major cracks at the crown of vaults, as well as along the head arches. The analysis of these patterns, combined with the results of numerical structural analyses, will allow to perform considerations regarding on-going settlements and/or deformations.

Regarding the generation of structural models, a simplification process of the triangular mesh models is required, since they are too irregular and extremely refined. This simplification process consisted in transforming the intrados surface of the vaults into NURBS. This was done by projecting lines onto the mesh derived from the point clouds (blue lines in Figs. 5 and 6a). These lines, which are complex polylines, have been described by simple regularized curves used to generate NURBS surfaces , as can be seen in Fig. 6b. In order to take into account the brick arrangements, the discretization of the intrados surface with regular curves has been done with lines that follow the bed joints (Fig. 6c) and that are subsequently translated normally to the intrados surface of a distance equal to the thickness of the vault (Fig. 6d). It is worth pointing out that at this moment the whole process of NURBS generation has been carried out with manual interpretation of intrados surfaces patterns and modelling of bricks courses, without any type of automation. In the future the research can be oriented toward experimenting semi-automated hybrid workflows for bricks pattern analysis and reconstruction via NURBS from point cloud data. In Fig. 7 it is possible to evaluate the level of approximation of the NURBS vaults from the reality-based point cloud data. The visualization shows the deviation maps projected on the 3D point cloud object in range colours for both the vaults pattern configurations, related to the colour-bar values (the gaussian curve besides the colour-bar displays the points deviation distribution and thus the global accuracy of the model). It represents the localization of the most simplified areas of the vaults surfaces and also indicates the extent of such approximation. In any case the surface modelling for both the NURBS models has been conducted with a mean accuracy of ±0.01 m (st.dev 0.005 m). Only in some cases the simplification exceeds 2 cm of tolerance. For the abutments a simplification has been assumed and performed in the NURBS modelling, in the connection with walls and arches, as visible from Fig. 7. Since in this case study it was not possible to directly measure the vault's thickness, this has been derived by observing the

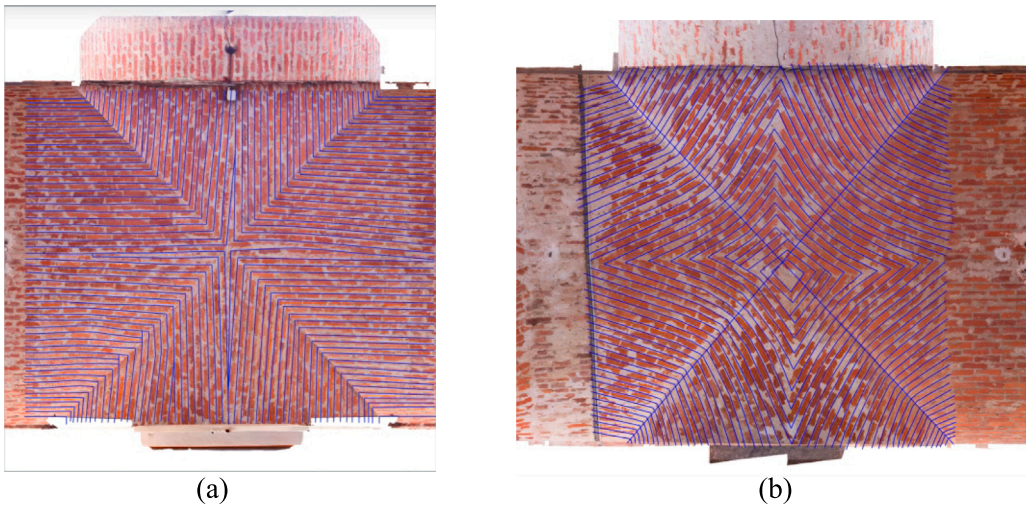

Fig. 5. Detection of bed joints on intrados surface of two vaults with radial (a) and diagonal pattern (b). (For interpretation of the references to colour in this figure, the reader is referred to the web version of this article.)

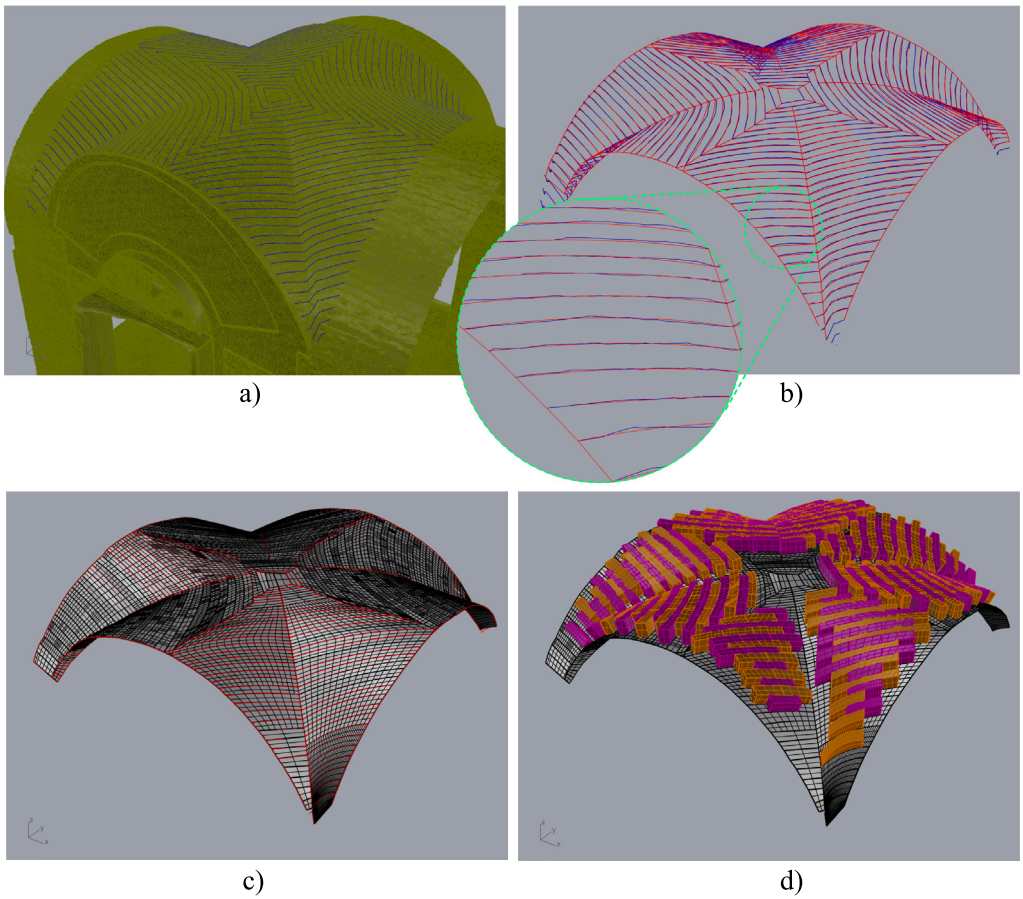

Fig. 6. Bed joints lines projected onto mesh (a), approximation process of construction lines for regularized sweep-surfaces (b), sweep surfaces of the vaults' intrados (c) and creation of 3D volumes corresponding to brick courses (d). (For interpretation of the references to colour in this figure, the reader is referred to the web version of this article.)

type of employed bricks and their orientation, as well as by supposing that bricks are layed in a single layer.

The two vaults that have been chosen as objects of the FE analyses are vault number 19 of block 1 and vault number 10 of block 2 (Fig. 3). This choice has been made because the vaults of blocks 1 and 2 are very similar in size and shape, whereas the vaults of block 3 differ greatly from a geometrical point of view from the others. Therefore, the main difference between the chosen vaults is the brick arrangement. Moreover, these two vaults show the least amount of existing cracks, which could mean that the shape of the intrados has not changed significantly over time due to support settlement (Fig. 8). In order to isolate the two vaults and perform FE analyses on them, confinement structures were taken into consideration. The front arch and lateral arches, as well as the back wall, have been modelled. The thickness of the front arch has been easily measured from the survey of the facade, whereas the thickness of the lateral confinement arches has

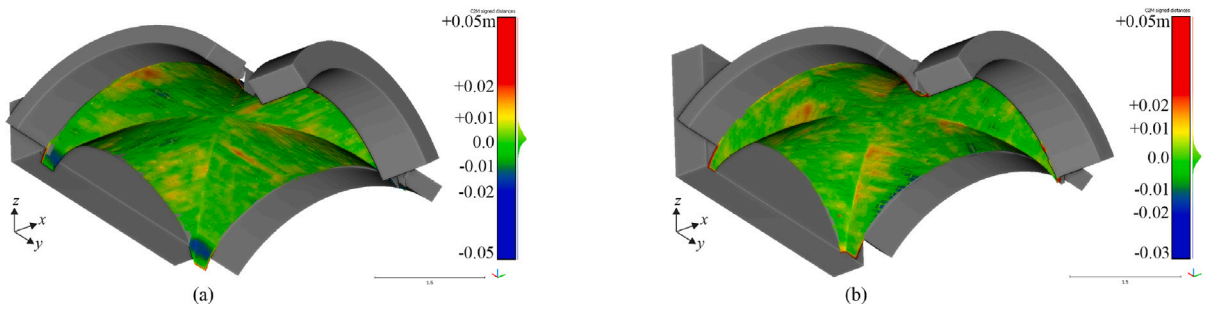

Fig. 7. Deviation analysis maps between starting 3D point cloud and final NURBS model (C2M algorithm, CloudCompare) for: (a) radial courses and (b) diagonal courses. Distances in (m) are related to colour ramp and distributed as shows the gaussian on the right side. (For interpretation of the references to colour in this figure, the reader is referred to the web version of this article.)

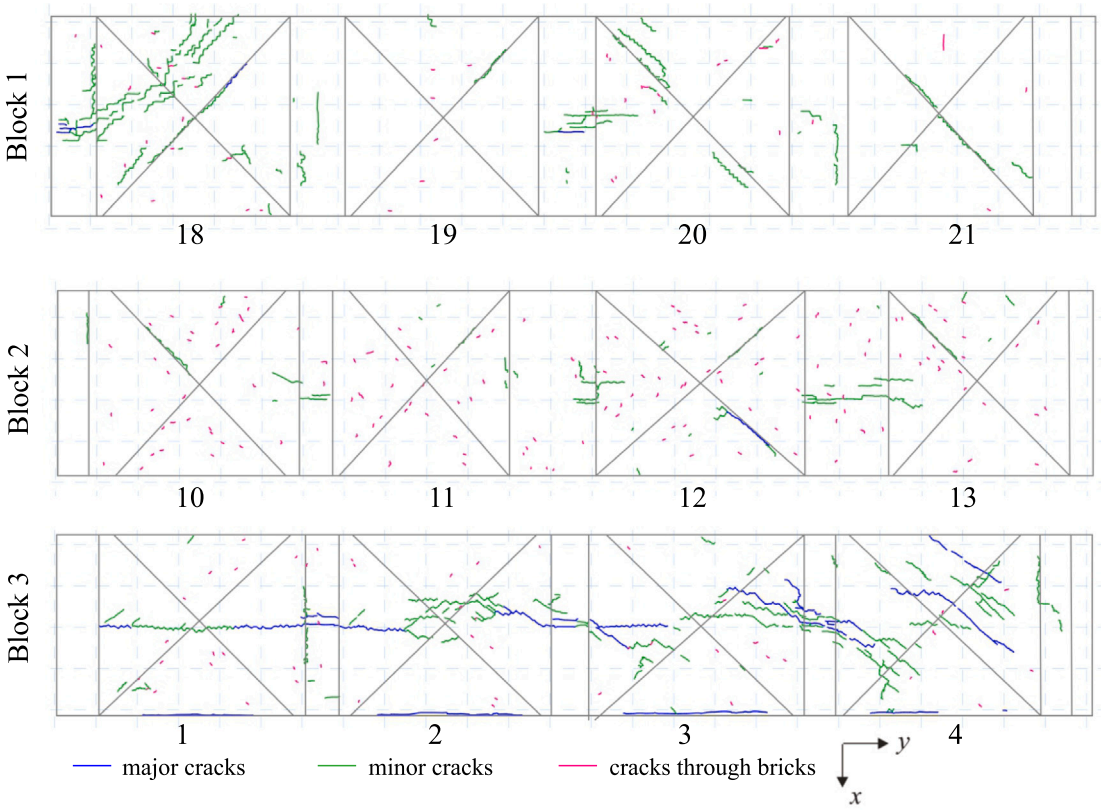

Fig. 8. Detection of crack patterns on the vaults intrados surfaces. (For interpretation of the references to colour in this figure, the reader is referred to the web version of this article.)

been estimated by observing the brick arrangements from the intrados: as a matter of fact, it is clearly visible that some bricks on the lateral arches are positioned vertically, resulting in the arch thickness of about the length of one brick (about 25 cm).

5. Reality-based finite element block model

Fig. 9 shows a plan view of the two vaults that have been chosen as objects of the FE analyses, with radial and diagonal brick patterns, respectively. The FE analyses have been performed in Abaqus®. The detailed geometric models described in the previous section have been used to generate FE micro-models, in which every masonry unit is described as a closed three-dimensional volume that must be perfectly adjacent to subsequent units, in order to generate zero-thickness interfaces between blocks, according to the simplified micro-modelling approach [27]. In particular, the detection of the surfaces into contact has been performed by exploiting the automatic algorithm of "contact-pair finding" implemented in Abaqus. The confining structures have been assumed as rigid back wall and deformable front and lateral arches able to transfer the applied loads.

The radial vault has a span of approximately 2.80 m and a rise of 0.81, whereas the diagonal vault spans over 2.95 m with the same rise. The discretization of the vault's geometry is performed by taking into account the actual distribution of bed joints, as in Fig. 5. Each resulting block therefore accounts for the brick dimensions (on average 6.5 × 13 × 25 cm) plus half the thickness of the mortar joints. Because of the irregular thickness of joints, these blocks show a quite large variability in shape and dimensions. In the absence of data concerning the mechanical characterization of the existing masonry material, the mechanical properties of blocks are those suggested in [28] for historic brick masonry, i.e., $\rho = 1800$ kg/m^3, E = 1200 MPa, $\nu = 0.2$. Interfaces are characterized by frictional tangential behaviour, with friction coefficient $\mu = 0.5$, and a very high stiffness value $k_n = 5 \cdot 10^9$ N/m^3 in compression to simulate a quasi-rigid normal contact [12]. The mass of an infill 13 cm-thick at the vault's crown, with a material density equal

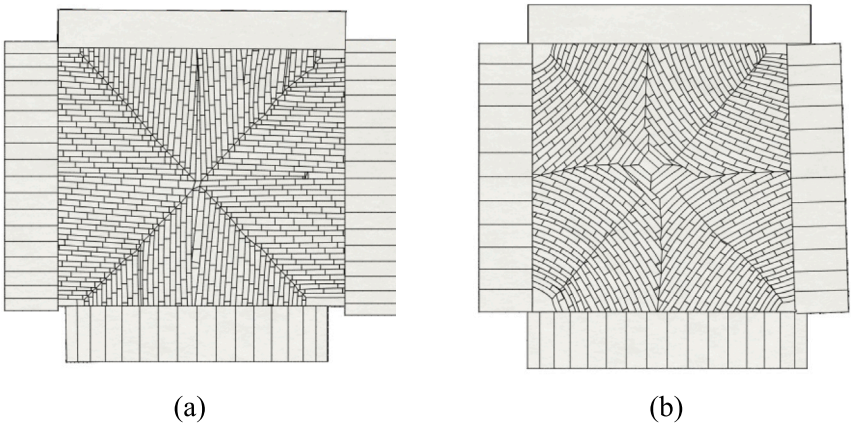

Fig. 9. Geometric model for FE analyses: radial (a) and diagonal pattern (b).

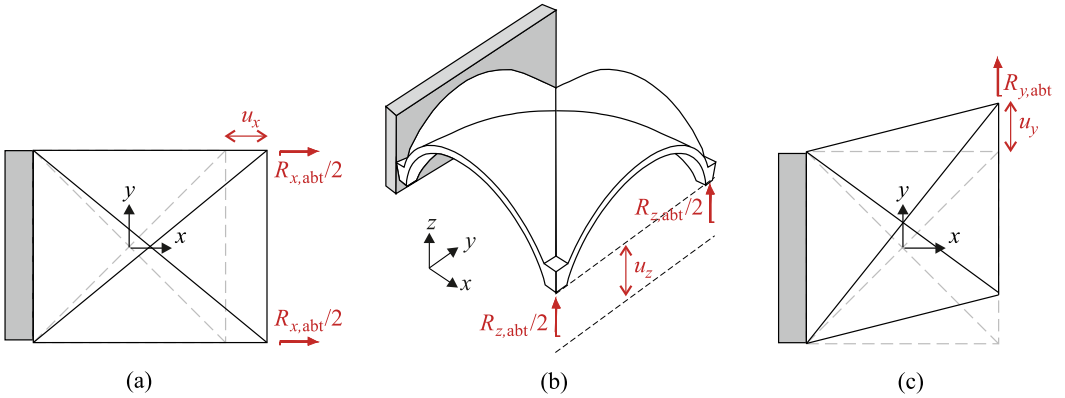

Fig. 10. Scheme of the imposed displacements and measured reaction forces at the abutments: opening (a), vertical (b) and shear (c) settlement.

to 900 kg/m^3, is taken into account and applied as vertical nodal forces on the nodes of the extrados surface.

The vaults are subject to their self-weight and to a settlement of the abutments. Three kinds of settlement are applied: a horizontal settlement of two abutments in x direction, resulting in an opening (O) mechanism (Fig. 10a); a horizontal settlement of two abutments in y direction, resulting in a shear (S) mechanism (Fig. 10b); a vertical (V) settlement of two abutments, that mimics subsidence of the pillars of the portico (Fig. 10c). It is noteworthy to remark that the masonry pillars are not modelled, assuming the hypothesis that they are able to transfer the lateral loads from their base to their head without experiencing premature failure or any deformation.

6. Results

This Section presents the numerical results obtained for imposed opening, vertical and shear settlements, respectively. Moreover, for the last type of settlement, a comparison with the results obtained on vaults of ideal geometry is commented on. The vaults of ideal geometry represent an ideal case, characterized by similar overall dimensions as the Vicoforte vaults (same span and rise-to-span ratio, but characterized by a perfect macro and micro geometry, i.e., modular bricks, regular pattern, perfect symmetry and curvature.

6.1. Opening settlement

The test is performed by moving the abutments of the vault and boundary arches in the x-direction, in order to simulate the overturning of the external pillars of the portico (Fig. 10a). Fig. 11 reports the deformed shapes, which allow to observe quite similar collapse mechanisms in the two considered vaults. The lateral confinement arches develop in both cases a three-hinge mechanism, one at the key and two near the abutments. The two vaults also show similar collapse shapes and crack patterns. A central hinge is formed at the crown of the vaults (blue line in Fig. 11). This crack is not perfectly parallel to the front arch, but follows the irregularity of the masonry apparatus. In both vaults, a detachment of the caps from the front arch and confinement wall is visible, being more evident in the radial vault (red line in Fig. 11). Both vaults also show a local failure at the key of the caps adjacent to the lateral arches. However, the diagonal vault experiences sliding of some bricks, whereas the radial vault undergoes the collapse of a larger portion of one cap. It is possible to notice how the lateral arches deform almost independently from the vaults, meaning that the tangential forces between the arches and the vaults' head arches are not significant.

Fig. 12 plots the load–displacement curves in the case of opening settlement for the two considered masonry patterns. The curves are built by plotting the horizontal thrusts at the abutments divided by the self-weight of the structure W (vault + boundary arches + abutments), versus the horizontal displacement of the moving supports u_x divided by the span of the vault L. Fig. 12a reports the total horizontal reaction force (sum of vault + lateral arches + front arch) at the moving abutments, while Fig. 12b shows the reaction force at the vault's abutments only (black lines) and at the boundary arches' abutments only (red lines). The activation of a global or local failure mechanism is identified as the point corresponding to a sudden increase of the differential vertical displacement Δu_z between two control nodes (highlighted by yellow dots in Fig. 11), meaning that the bricks start sliding (Fig. 13). These points are shown in the curves with a square or circle marker for radial and vertical pattern, respectively.

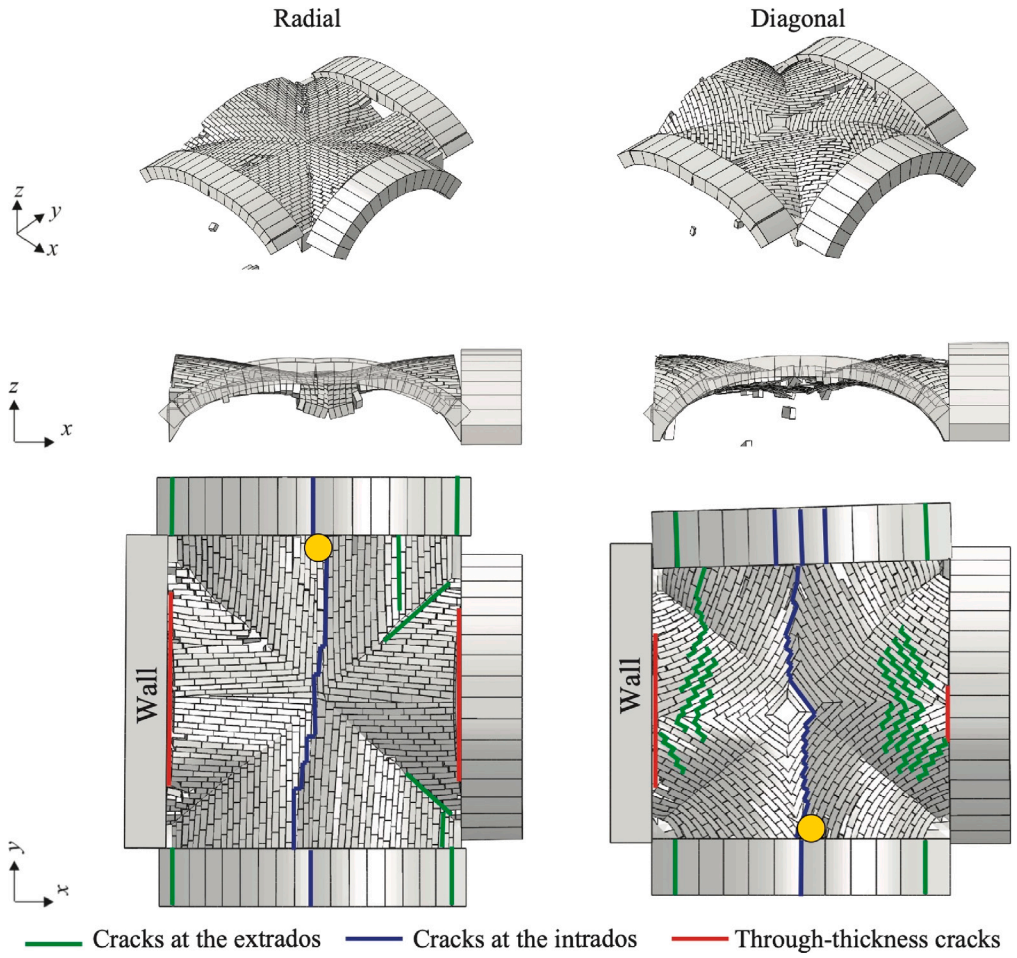

Fig. 11. Deformed shapes for opening settlement: axonometric view (first row), x–z plane view (second row), extrados plan view (third row). (For interpretation of the references to colour in this figure, the reader is referred to the web version of this article.)

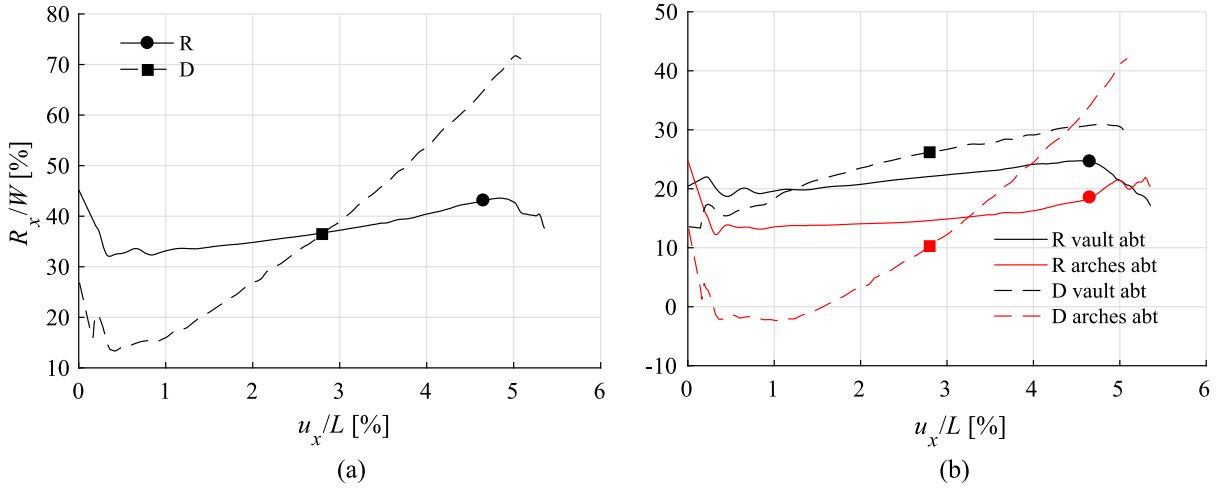

Fig. 12. Normalized total reaction forces R_x (a) and reaction forces at the vault's and boundary arches' abutments (b) versus normalized imposed displacement for opening settlement. (For interpretation of the references to colour in this figure, the reader is referred to the web version of this article.)

In the radial (R) vault, the collapse of one cap (circle marker) produces an abrupt variation of the slope of the curves, especially in the case of the horizontal thrust at the vault's abutments (Fig. 12b). This is due to the fact that the local collapse of one cap involves a quite large part of the structure. On the contrary, in the diagonal vault (D), no major collapses are visible, but the sliding of several blocks takes place at the key of two caps at an earlier stage with respect to the radial vault. These failures do not change the trend of the load–displacement curves, but still represent a hazard in terms of safety of the structure. If these points are considered as a measure of the vault displacement capacity, Fig. 12 evidences that the radial vault has the largest displacement capacity, being 1.62 times greater than the diagonal vault. Note that

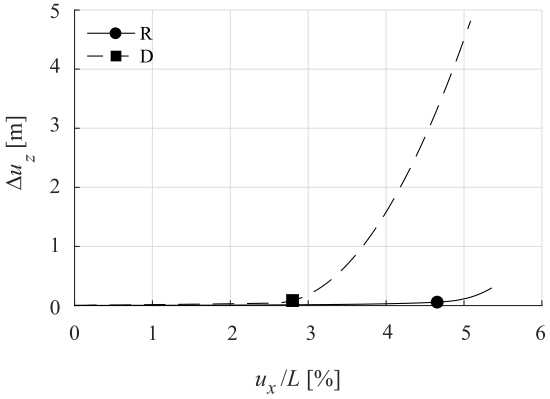

Fig. 13. Differential vertical displacement versus normalized imposed displacement for opening settlement.

the value of normalized horizontal thrust at the beginning of the curves is lower in the case of the diagonal vault: this is probably not entirely attributable to the block arrangements, but also to the overall shape and initial deformation of the vaults.

6.2. Vertical settlement

This test is performed by imposing a vertical settlement in the z-direction to the abutments of the vault and boundary arches, in order to simulate the subsidence of the external pillars of the portico (Fig. 10b). As in the previous test, the abutments of the front arch, the lateral arches and the vault are moving simultaneously. Conversely, the other abutments and the confinement wall are kept fixed. The deformed shapes are shown in Fig. 14 and allow to observe that both vaults experience damage in the caps adjacent to the lateral arches. As in the case of opening settlement, the radial vault shows a more global mechanism, showing the creation of three parallel cracks in the y-direction and the collapse of the central part of the structure. Conversely, the diagonal vault shows partial collapse along the groins and a longitudinal crack develops in the y-direction along the entire vault, clearly visible from the intrados view. The lateral confinement arches develop in both cases a two-hinge mechanism, consisting in two hinges at the haunches. The radial vault experiences a detachment of the caps from the confinement wall and front arch, which remains undeformed. On the contrary, the diagonal vault remains in contact with the front arch and causes its out-of-plane deformation. Both vaults also show a local failure at the key of the caps adjacent to the lateral arches. However, the diagonal vault undergoes the loss of only few bricks at an earlier stage of the test, whereas the radial vault experiences the collapse of a larger portion of two caps at a later stage. It is possible to notice how, also in the case of vertical settlement, the lateral arches deform independently from the vaults, meaning that the tangential forces between the arches and the vaults' head arches are not significant.

In Fig. 15, the load–displacement curves in the case of vertical settlement for the two considered masonry patterns are shown. Reaction forces and imposed settlements are normalized with respect to the structure's self-weight W and span L, respectively. Fig. 15 reports the total vertical reaction force (sum of vault + lateral arches + front arch) at the moving abutments (a) and at the vault's and boundary arches' abutments only (b). The activation of a partial or global collapse is identified with the same criterion adopted for the opening settlement and highlighted in all curves with a square or circle marker.

In the radial vault, the collapse of two lateral caps causes the global failure of the vault and is clearly recognizable in the abrupt variation of the slope of the curves, especially in the case of the vertical reaction force at the vault's abutments (Fig. 15b). Conversely, the diagonal vault does not experience a major collapse; several blocks start sliding and falling at the key of two lateral caps at an earlier stage with respect to the radial vault. These local failures occur at a value of normalized imposed displacement of about 4% (square marker). However, there are no major changes in the trend of the load–displacement curve at this point. The curves referred to the vault's and arches' abutments considerably vary their slope at a value of imposed vertical displacement u_z/L of about 15% (similar to the radial vault), possibly implying the beginning of a global collapse mechanism. Nevertheless, as previously stated, the fall of a limited number of blocks can still represent a hazard, even though the structure is still globally stable. If the values of imposed displacement corresponding to the markers are considered as a measure of the vaults' ductility, the radial vault shows the largest displacement capacity, being 3.5 times greater than the diagonal vault.

6.3. Shear settlement

The test is performed by moving two abutments of the vault and boundary arches in the y-direction (Fig. 10c). The deformed shapes in Fig. 16 show that the two vaults experience quite different collapse shapes; however, in both cases only a partial collapse of the structure can be observed. In the case of the radial vault, a typical diagonal crack along the groins can be seen, as well as a hinge at the key of one cap, parallel to the orientation of the bed joints. The collapse of one cap can be observed. In the case of the diagonal vault, damage along the groins is not visible, and cracks develop normally to the groins. In this case, the local collapse of the structure involves two caps and is mainly concentrated along one groin. It is noteworthy to point out that the local collapses occur in quite different regions of the vaults, depending on the considered brick arrangement. The obtained results can be qualitatively compared with the ones of a previous study carried out on cross vaults of ideal geometry [12]. The two ideal vaults have similar macro geometry as the Vicoforte ones (span = 3.1 m, rise = 1.175 m), the same boundary condition as the real vaults, but differ in the static load since the mass of infill was not taken into account in the ideal case. Despite this difference, the cited study demonstrated that the presence of infill does not significantly modify the overall collapse shape, but only influences the vault capacity and ductility. The ideal vaults described in [12] show the same qualitative collapse shapes as the Vicoforte vaults. This confirms the fact that, despite the differences in macro-geometry (overall shape and dimensions) of the two vaults in Vicoforte, the two different brick arrangements are the main cause for the propagation of specific crack patterns and resulting collapse mechanisms, as already demonstrated in other numerical and experimental studies [29,30].

Fig. 17 plots the horizontal thrusts in the y direction at the abutments versus the horizontal displacement of the moving supports u_y for the Vicoforte and ideal vaults for comparison [12]. The two vaults in Vicoforte show similar values of peak force R_{max} and of initial stiffness K_{tan} (percentage differences around 20%). Local collapses are highlighted on the load–displacement curves with yellow markers. In the radial vault the local collapse of one cap occurs in the post-peak branch in correspondence of an abrupt variation of the slope of the curve. Conversely, in the diagonal vault the local collapse, induced by sliding of few bricks, occurs when the reaction force reaches its peak value. If these local collapses are considered as a measure of the vault displacement capacity u_c, the radial vault has the largest displacement capacity being almost 6 times greater than the diagonal vault. Conversely, the two vaults show very similar ductile behaviour, being the ductility evaluated as the ratio between the imposed displacement corresponding to a decrease of 80% of the peak force value (u_{80}) and the displacement corresponding to 60% of R_{max} (u_{60}). A comparison of critical quantities is reported in Table 2.

The different load condition that real and ideal vaults withstand does not allow a thorough quantitative comparison between the results obtained for Vicoforte and ideal vaults. Nevertheless, a qualitative comparison between the load–displacement curves (Fig. 18) and critical quantities (Table 2), as well as the crack patterns (Fig. 19) allows to outline the following comments:

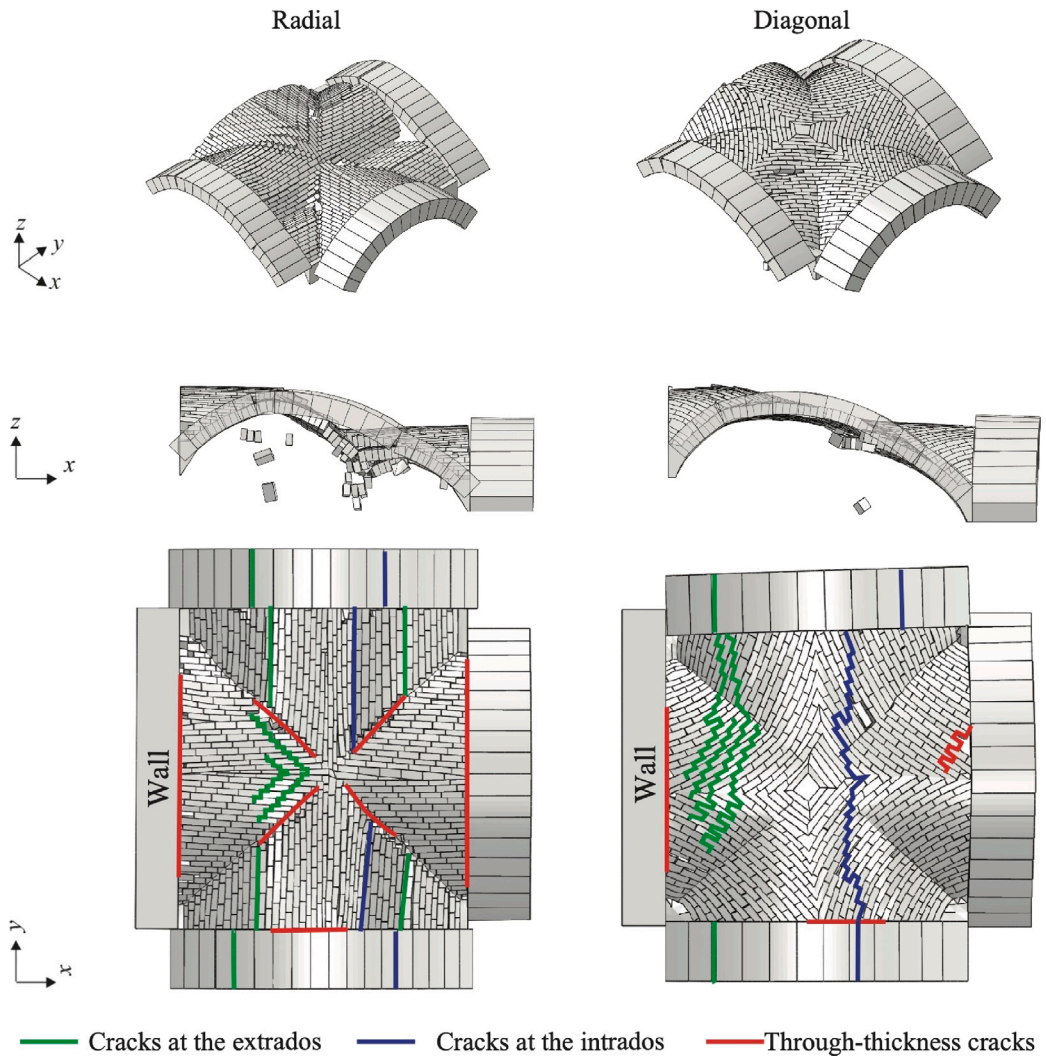

Fig. 14. Deformed shapes for vertical settlement: axonometric view (first row), x–z plane view (second row), extrados plan view (third row). (For interpretation of the references to colour in this figure, the reader is referred to the web version of this article.)

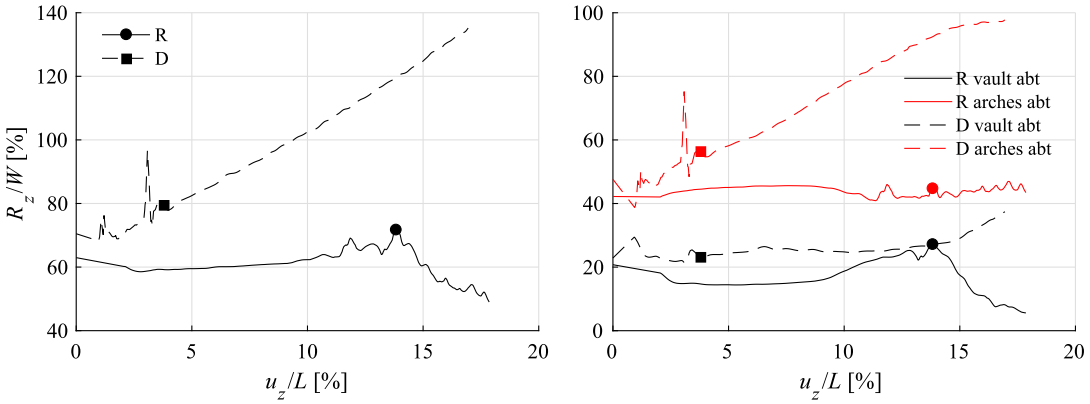

Fig. 15. Normalized total reaction forces R_z (a) and reaction forces at the vault's and boundary arches' abutments (b) versus normalized imposed displacement for vertical settlement. (For interpretation of the references to colour in this figure, the reader is referred to the web version of this article.)

- The two ideal vaults only differ from each other for the brick pattern, therefore the differences in critical quantities between radial and diagonal vaults are certainly due to the micro-geometry;
- The two real vaults in Vicoforte have different brick arrangement and similar, but not equal macro-geometry, therefore differences in critical quantities cannot be attributed only to the brick pattern but are also related to the influence of the overall vault dimensions (i.e., different rise-to-span-ratio and different self-weight). These geometric irregularities and imperfections are responsible for the higher percentage difference between diagonal and radial critical quantities in real vaults;

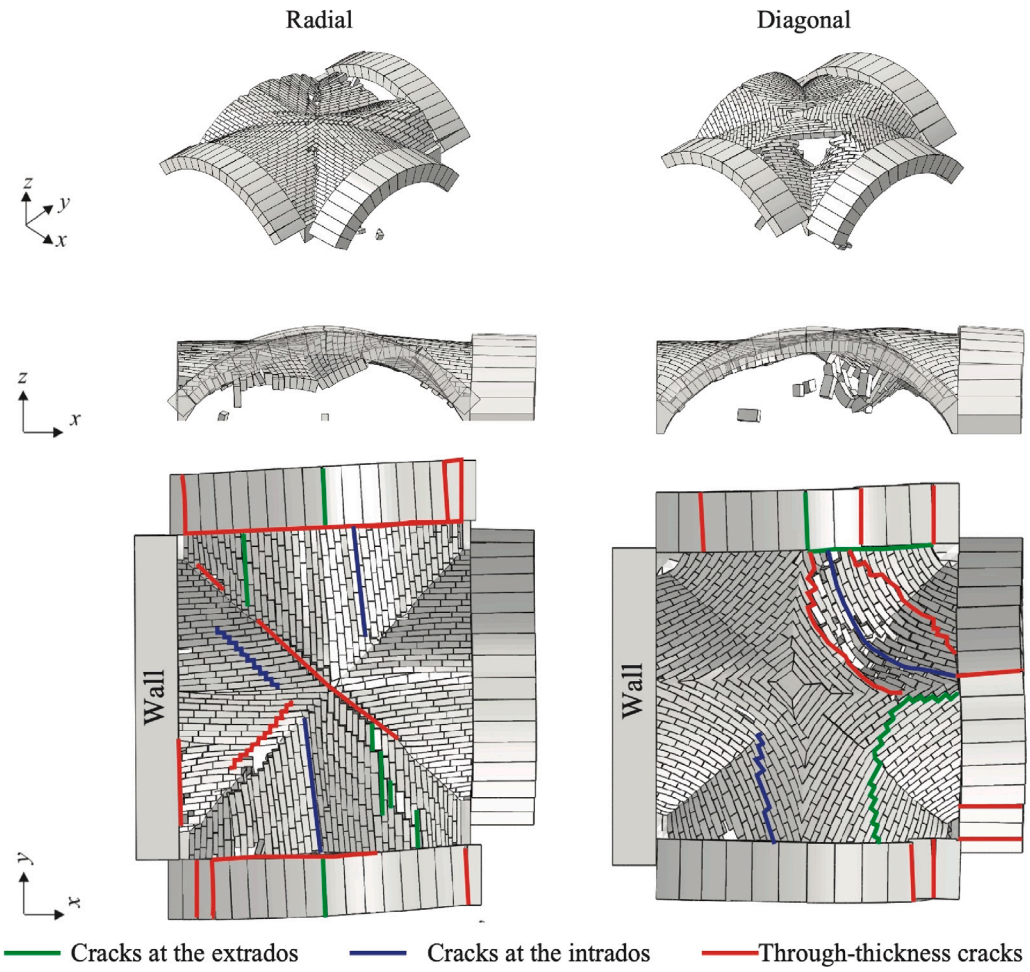

Fig. 16. Deformed shapes for shear settlement: axonometric view (first row), x–z plane view (second row), extrados plan view (third row). (For interpretation of the references to colour in this figure, the reader is referred to the web version of this article.)

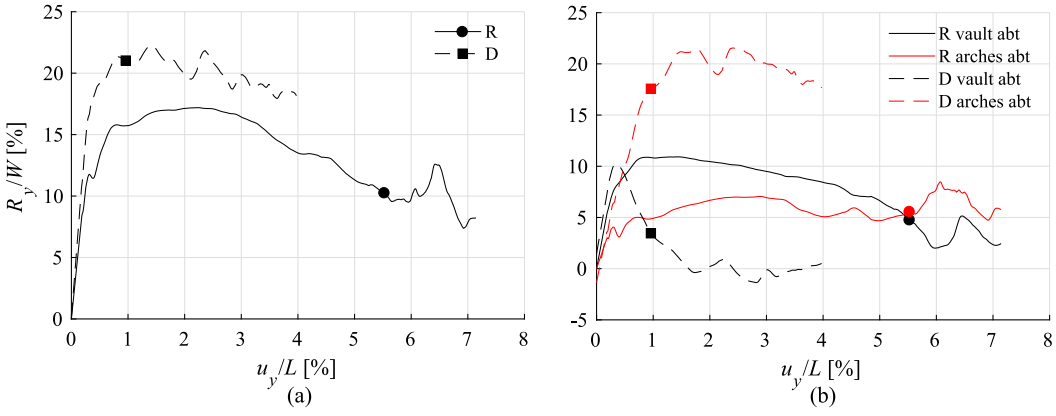

Fig. 17. Normalized total reaction forces R_y (a) and reaction forces at the vault's and boundary arches' abutments (b) versus normalized imposed displacement for shear settlement. (For interpretation of the references to colour in this figure, the reader is referred to the web version of this article.)

- the higher capacity of the real vaults with respect to the ideal ones can be attributed to the stabilizing effect of the infill (as already demonstrated in [12]), which was not considered in the ideal setup;
- in both real and ideal vaults the radial pattern involves lower peak force and higher displacement capacity with respect to the diagonal one.
- the crack pattern of ideal vaults and reality-based vaults present some similarities, as depicted in Fig. 19. Vaults with the same brick arrangement (i.e. reality-based *radial* and ideal *radial*) develop a consistent crack pattern, even though their macro-geometrical dimensions and/or overall shapes differ; this can denote that the evolution of cracks is influenced greatly by the micro-geometrical aspects, such as the brick pattern.

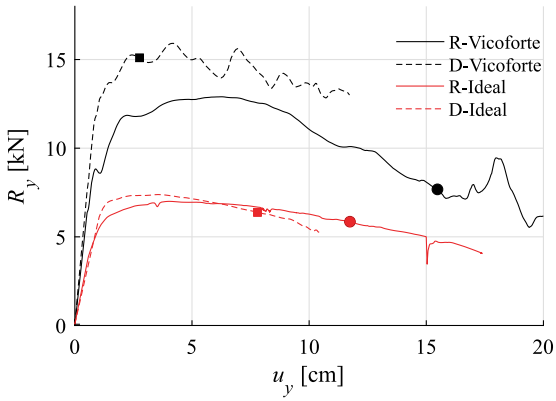

Fig. 18. Total reaction force vs. imposed displacement for Vicoforte and ideal vaults. (For interpretation of the references to colour in this figure, the reader is referred to the web version of this article.)

6.4. Interpretation of surveyed crack patterns

The comparison between detected and numerical crack patterns allows some considerations about possible on-going settlements and/or displacements of the structures to be outlined.

Table 2
Table of critical quantities for Vicoforte and ideal vaults for shear settlement.

Case study	Pattern	R_{max} [N]	u_c [m]	K_{tan} [N/m]	u_{80}/u_{60} [–]
Vicoforte	Radial	12 891	0.1613	1 217 770	15.18
	Diagonal	15 913	0.0276	1 451 315	17.35
	Δ=(D-R)/R [%]	23.44	−82.89	19.18	14.30
Ideal	Radial	6931	0.118	658 815	18.82
	Diagonal	7314	0.078	581 957	12.31
	Δ=(D-R)/R [%]	5.53	−33.90	−11.67	−34.59

For instance, in Fig. 8 Block 1 shows cracks mainly along the groins: this crack pattern is consistent with the ones obtained from the numerical models, where the radial vault is always interested by cracks along the groins whichever the type of settlement. Block 2 (diagonal cross vaults) appears to be the less damaged, showing mostly minor cracks. Conversely, Block 3 shows a crack pattern that could be related to an opening mechanism for vaults 1 to 3 and also a shear mechanism for vault 4. Considering that these vaults are built with a diagonal pattern, vaults 1–3 show a typical longitudinal crack at the key of the vault, as well as a crack between one cap of the vault and the front arch on the facade: this crack pattern can be related to an opening mechanism, as can be seen in Fig. 11. Vault 4 shows a crack pattern that can be associated with a shear/opening mechanism, with diagonal cracks along principal joints (typical of a shear deformation, as in Fig. 16) and a crack between the front arch of the facade and the vault's

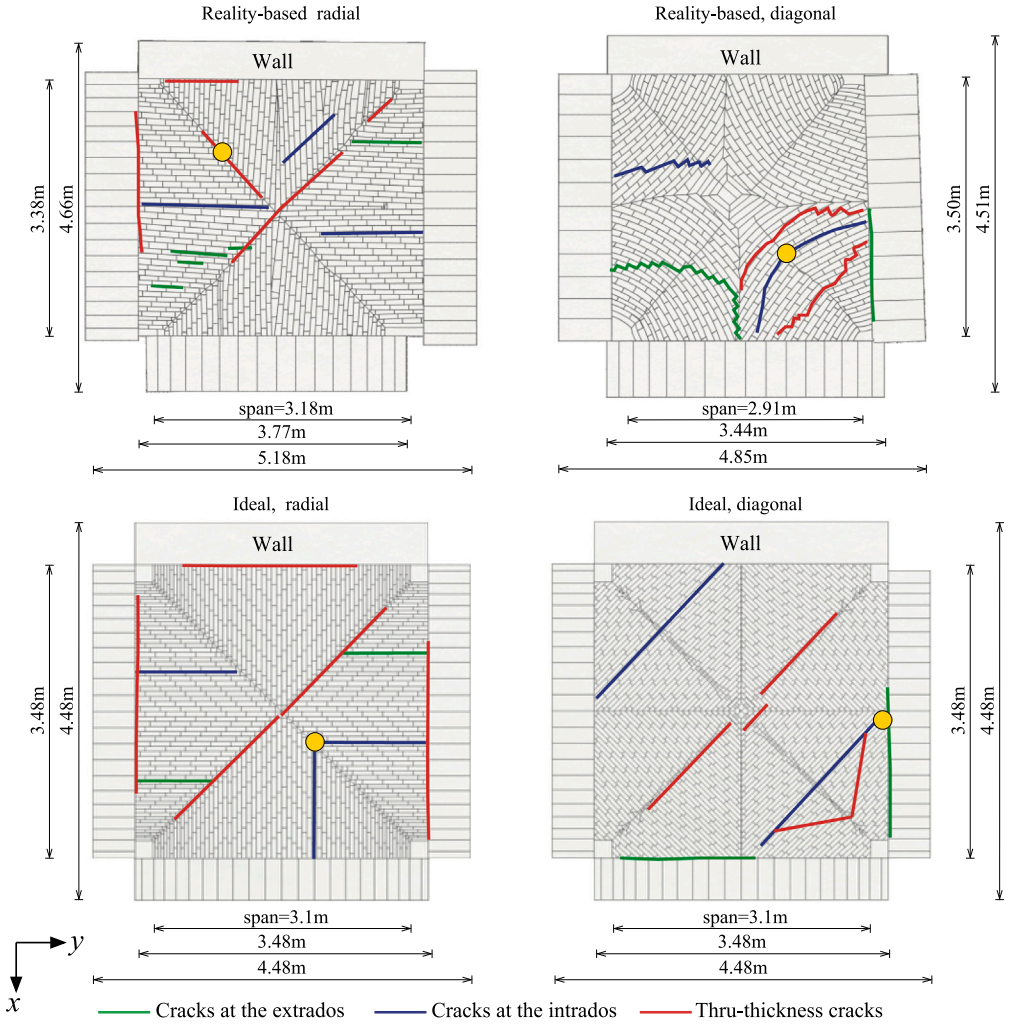

Fig. 19. Overall dimensions and crack patterns for shear settlement for Ideal vaults and Reality based vaults. The yellow dots represent the location of a first local collapse. (For interpretation of the references to colour in this figure, the reader is referred to the web version of this article.)

cap, as in an opening mechanism. By looking at the surveyed cracks and the results of the numerical models, it can be hypothesized that the pillars between vaults 1–2, 2–3 and 3–4 have moved outwards, as in an over-turning mechanism. In order to evaluate the actual settlement (if any) that generated these cracks, it could be useful to perform a geometric deformation analysis of the entire structural system (pillars, walls, foundations), however this is out of the scope of this paper.

7. Conclusions

In this paper, a methodological approach to develop reality-based finite element models of masonry vaults has been proposed and tested on a real case study. Specifically, two vaults belonging to the porch of the Palazzata di Vicoforte in Piedmont, Italy, characterized by similar macro-geometry but different masonry patterns, have been considered. The detailed macro- and micro-geometries of the vaults have been obtained from a 3D campaign with LiDAR acquisitions and photogrammetric survey, which allowed to obtain dense point clouds subsequently adopted in the as-built modelling pipeline, finally delivering accurate NURBS for the generation of the Finite Element Model. The brick pattern is carefully manually modelled according to a FE micro-modelling strategy, in order to take into consideration its influence on the structural behaviour of the vaults.

Further researches can be planned in the direction of the evaluating the influence of the level of simplification in micro-modelling strategy in the reliability of results estimation (i.d a greater approximation of the surfaces imperfections based on lower accuracy 3D data).

The vaults' response under opening, vertical and shear settlements is numerically analysed. The two vaults that have been studied show quite different behaviour under the same imposed settlement in terms of collapse shapes and displacement capacity. Even though this cannot be entirely attributed to the different brick arrangements of the two vaults (the actual macro-geometry of the structures comes into play), it is noteworthy to point out that the obtained results are consistent, from a qualitative point of view, with the results obtained in the study of ideal vaults in [12] subjected to shear settlement.

The adopted reality-based approach, besides making possible the definition of highly detailed structural models, also allows the accurate detection of existing cracks and damage. This further information could be useful in the diagnosis of the structural health, since it allows to spatially 3D relate the observed crack pattern with a specific load condition. Moreover, it could be used to develop structural models able to account also for the deformed structural configuration.

Further studies on different grade of surface simplification are also potentially significant, in the direction of assessing the suitability of different type of 3D point data for structural assessment, derived from rapid mapping technologies acquisition (e.g. SLAM-based data from mobile scanners, 360° cameras, etc.).

Additional studies are surely needed to test and evaluate new workflows for reducing the great effort in the blocks pattern modelling and cracks interpretation processes, e.g., by adopting block pattern generating algorithms based on masonry textures samples, as in [18–20], or by applying a discretization method that takes into consideration only the type of pattern (principal direction of bed joints) but does not exactly replicate the position of each block. Specifically for automation approaches, further developments to simplify the modelling process involve innovative semi-automated assisted procedures based on Visual Programming Languages (VPL) for converting point clouds in 3D surfaces and semantically-featured parametric objects [31]. On the other hand, also for the crack pattern recognition and extraction, recent studies increasingly support automation via image-based processing and AI contributes [32,33]. By doing so, it would be possible to still take into consideration the role of micro- and macro-geometry, with a simplified but more efficient approach.

CRediT authorship contribution statement

Marco Alforno: Conceptualization, Data curation, Formal analysis, Investigation, Methodology, Validation, Visualization, Writing – original draft, Writing – review & editing. **Alessia Monaco:** Conceptualization, Methodology, Supervision, Writing – original draft, Writing – review & editing. **Fiammetta Venuti:** Investigation, Methodology, Supervision, Visualization, Writing – original draft, Writing – review & editing, Conceptualization, Formal analysis. **Chiara Calderini:** Conceptualization, Supervision, Writing – original draft, Writing – review & editing. **Giulia Sammartano:** Data curation, Visualization, Writing – original draft, Writing – review & editing, Resources, Software. **Giacomo Patrucco:** Data curation, Writing – original draft, Writing – review & editing, Resources, Software. **Antonia Spanó:** Data curation, Resources, Software.

Declaration of competing interest

The authors declare that they have no known competing financial interests or personal relationships that could have appeared to influence the work reported in this paper.

Acknowledgements

This article is a revised and expanded version of work presented in IWSS2023 conference, titled: 'Reality-Based FE Block Models of Masonry Cross Vaults: A Real Case Study' [34]

References

[1] Castellazzi G, D'Altri A, Bitelli G, Selvaggi I, Lambertini A. From laser scanning to Finite Element analysis of complex buildings by using a semi-automatic procedure. Sensors 2015;15:18360–80.
[2] Korumaz M, Betti M, Conti A, Tucci G, Bartoli G, Bonora V, et al. An integrated Terrestrial Laser Scanner (TLS), Deviation Analysis (DA) and Finite Element (FE) approach for health assessment of historical structures. A minaret case study. Eng Struct 2017;153:224–38.
[3] Angjeliu G, Cardani G, Coronelli D. A parametric model for ribbed masonry vaults. Autom Constr 2019;105:102785.
[4] Ceravolo R, Invernizzi S, Lenticchia E, Matteini I, Patrucco G, Spanó A. Integrated 3D mapping and diagnosis for the structural assessment of architectural heritage: Morano's parabolic arch. Sensors 2023;23:6532.
[5] Remondino F, Nocerino E, Toschi I, Menna F. A critical review of automated photogrammetric processing of large datasets. Int Arch Photogramm Remote Sens Spatial Inf Sci 2017;XLII-2/W5:591–9.
[6] Kersten T, Lindstaedt M. Potential of automatic 3D object reconstruction from multiple images for applications in architecture, cultural heritage and archaeology. Int J Herit Digit Era 2012;1:399–420.
[7] Fino MD, Galantucci R, Fatiguso F. Condition assessment of heritage buildings via photogrammetry: A scoping review from the perspective of decision makers. Heritage 2023;6:7031–66.
[8] Sánchez-Aparicio L, Pozo SD, Ramos L, Arce A, Fernandes F. Heritage site preservation with combined radiometric and geometric analysis of TLS data. Autom Constr 2018;85:24–39.
[9] Adamopoulos E, Rinaudo F. Close-range sensing and data fusion for built heritage inspection and monitoring—A review. Remote Sens 2021;13:3936.
[10] Sammartano G, Spanò A. High scale 3d modelling and orthophoto of curved masonries for a multipurpose representation, analysis and assessment. Int Arch Photogramm Remote Sens Spatial Inf Sci 2017;42:245–52.
[11] Spanó A, Patrucco G, Sammartano G, Perri S, Avena M, Fillia E, et al. Digital twinning for 20th century concrete heritage: HBIM cognitive model for torino esposizioni halls. Sensors 2015;23:4791.
[12] Alforno M, Venuti F, Monaco A, Calderini C. Numerical investigation of the influence of constructive aspects on the structural behaviour of masonry cross vaults. Int J Archit Herit 2021;17:868–91.
[13] Foti D, Vacca V, Facchini I. DEM modeling and experimental analysis of the static behavior of a dry-joints masonry cross vaults. Constr Build Mater 2018;170:111–20.
[14] Boni C, Ferretti D, Lenticchia E. Effects of brick pattern on the static behavior of masonry vaults. Int J Archit Herit 2021;16:1–21.
[15] Guarnieri A, Fissore F, Masiero A, Di Donna A, Coppa U, Vettore A. From survey to FEM analysis for documentation of built heritage: The case study of villa revedin-bolasco. Int Arch Photogramm Remote Sens Spatial Inf Sci 2017;42:527–33.

[16] Funari M, Hajjat A, Masciotta M, Oliveira D, Lourenco P. Parametric scan-to-fem framework for the digital twin generation of historic masonry structures. Sustainability 2021;13:11088.
[17] Selvaggi I, Bitelli G, Serantoni E, Wieser A. Point cloud dataset and FEM for a complex geometry: the San Luzi bell tower case study. Int Arch Photogramm Remote Sens Spatial Inf Sci 2019;XLII-2/W11:1047–52.
[18] Shaqfa M, Beyer K. A virtual microstructure generator for 3D stone masonry walls. Eur J Mech A Solids 2022;96.
[19] Pantoja-Rosero B, Saloustros S, Achanta R, Beyer K. Image-based geometric digital twinning for stone masonry elements. Autom Constr 2023;145.
[20] Pereira M, D'Altri A, de Miranda S, Glisic B. Automatic multi-leaf nonperiodic block-by-block pattern generation and computational analysis of historical masonry structures. Eng Struct 2023;283.
[21] Beltramo S. Le botteghe dei pellegrini nel Piemonte Sabaudo tra XVI e XVII Secolo: i Santuari di Vicoforte e di Oropa. In: D. Calabi SB, editor. Il mercante patrizio: palazzi e botteghe nell'Europa del Rinascimento. Milano: Mondadori; 2008, p. 257–82.
[22] Tang P, Huber D, Akinci B, Lipman R, Lytle A. Automatic reconstruction of as-built building information models from laser-scanned point clouds: A review of related techniques. Autom Constr 2010;19:829–43.
[23] Barazzetti L, Banfi F, Brumana R, Previtali M, Roncoroni F. BIM from laser scans…not just for buildings: NURBS-based parametric modeling of a medieval bridge. ISPRS Ann Photogramm Remote Sens Spatial Inf Sci 2016;III-5:51–6.
[24] Banfi F. BIM orientation: grades of generation and information for different type of analysis and management process. Int Arch Photogramm Remote Sens Spatial Inf Sci 2017;XLII-2/W5:57–64.
[25] Granshaw S. Photogrammetric terminology: fourth edition. Photogramm Rec 2020;35:143–288.
[26] Sacco G, Ferrero C, Battini C, Calderini C. Combined use of deformation and structural analysis for the structural damage assessment of heritage buildings: A case study in the Liguria region (Italy). Eng Fail Anal 2023;147.
[27] Lourenço P, Rots J, Blaauwendraad J. Two approaches for the analysis of masonry structures - micro and macro-modeling. Heron 1995;40:313–40.
[28] Rossi M, Calderini C, Lagomarsino S. Experimental testing of the seismic in-plane displacement capacity of masonry cross vaults through a scale model. Bull Earthq Eng 2016;14:261–81.
[29] Roselli F, Alforno M, Bertetto AM, Venuti F. Experimental investigation of the effect of brick pattern on the structural response of masonry arches and barrel vaults. Constr Build Mater 2023;368:130434.
[30] Boni C, Ferretti D, Lenticchia E, Tasora A. DEM modelling of masonry vaults: Influence of brick pattern and infill on stability during supports displacements. In: IASS symposium 2019 - 60th anniversary symposium of the international association for shell and spatial structures; structural membranes 2019 - 9th international conference on textile composites and inflatable structures, FORM and FORCE. 2019, p. 1555–62.
[31] Roman O, Avena M, Farella EM, Remondino F, Spanò A. A semi-automated approach to model architectural elements in scan-to-BIM processes. Int Arch Photogramm Remote Sens Spatial Inf Sci 2023;XLVIII-M-2-2023:1345–52.
[32] Loverdos D, Sarhosis V. Automatic image-based brick segmentation and crack detection of masonry walls using machine learning. Autom Constr 2022;140:104389.
[33] Katsigiannis S, Seyedzadeh S, Agapiou A, Ramzan N. Deep learning for crack detection on masonry façades using limited data and transfer learning. J Build Eng 2023;76:107105.
[34] Alforno M, Monaco A, Venuti F, Calderini C, Sammartano G, Patrucco G, et al. Reality-based FE block models of masonry cross vaults: A real case study. Lect Notes Civ Eng 2024;437:108–17.